RAA 2016 Vol. **16** No. **9**, 149 (8pp) doi: 10.1088/1674–4527/16/9/149
http://www.raa-journal.org *http://iopscience.iop.org/raa*

***R**esearch in*
***A**stronomy and*
***A**strophysics*

A new estimation of manganese distribution for local dwarf spheroidal galaxies

Men-Quan Liu[1,2] and Zhong-Xiang Wang[2]

[1] School of Physics and Space Science, China West Normal University, Nanchong 637009, China; *liumq@cwnu.edu.cn*
[2] Shanghai Astronomical Observatory, Chinese Academy of Sciences, Shanghai 200030, China

Received 2016 January 22; accepted 2016 June 3

Abstract The distribution of abundance for iron-peak elements in dwarf spheroidal galaxies (dSphs) is important for galaxy evolution and supernova (SN) nucleosynthesis. Nowadays, manganese (Mn) is one of the most observed iron-peak elements in local dSphs. Studies of its distributions allow us to derive and understand the evolution history of these dSphs. We improve a phenomenological model by a two-curve model including a new initial condition, that includes detailed calculations of SN explosion rates and yields. We compare the results with the observed Mn distribution data for three dSphs: Fornax, Sculpture and Sextans. We find that the model can describe the observed Fe and Mn distributions well simultaneously for the three dSphs. The results also indicate that the initial conditions should be determined by the low metallicity samples in the beginning time of the galaxies and the previous assumption of metellicity-dependant Mn yield of SNIa is not needed when a wide mass range of core-collapse SNe is included. Our method is applicable to the chemical evolution of other iron-peak elements in dSphs and can be modified to provide more detailed processes for the evolution of dSphs.

Key words: galaxies: dwarf — galaxies: individual (Fornax, Sculptor, Sextans) — galaxies: evolution — supernovae: general

1 INTRODUCTION

Local dwarf spheroidal galaxies (dSphs) are neighbors of our Milky Way with tens of them now known. They are considered to be interesting places to search for dark matter, since there is so little luminous matter in them (see e.g., Bhattacherjee et al. 2014; Tolstoy et al. 2009). Studies of element abundance in dSphs are not only important for our understanding of galaxy evolution, but also allow us to learn about nucleosynthesis, star formation history and even the early evolution of the universe (see e.g., Graziani et al. 2015). Due to their shallow gravitational potential well, supernova (SN) explosions can drive gas out of dSphs, which causes the gas in dSphs to decrease and thus limits star formation (i.e., so called "SNe feedback"). As a result there is little remaining gas in dSphs at present (Kirby et al. 2011b).

There are at least two advantages for us to study chemical evolution in local dSphs. Although dSphs have experienced complicated evolutionary histories, their chemical evolution is rather 'clear' compared to that of massive galaxies, which may have experienced mergers or material exchanges with other galaxies. The other advantage is that their stars may be observed individually and in detail, even for the farthest dSphs such as Leo I and Leo II, given their relatively short distances from us (Tolstoy et al. 2009). The Dwarf galaxy Abundance and Radial-velocity Team (DART) survey has obtained many accurate spectra of bright stars in dSphs (Helmi et al. 2006), and even detected some low abundant elements, such as iron-peak elements. In 2011, Kirby et al. (2011a) presented metallicity distribution functions for the central regions of eight local dSphs based on spectral synthesis of iron absorption lines. In 2012, North et al. (2012, hereafter N12) reported their results of Mn abundance for a large number of stars in the dSphs Sculptor and Fornax, and for a few in the dSphs Sextans and Carina. Their results have made a significant improvement in the sample numbers of local dSphs.

For example, there were only a few stars whose Mn abundance was measured for dSphs Fonax and Sculptor in 2003 (Shetrone et al. 2003). The progress thus provides a possibility to check theoretical models for the Local Group, including the evolution of dSphs, the nucleosynthesis yield and the explosion rate of SNe.

While the chemical evolution of dSphs was investigated by many authors (e.g., Lanfranchi & Matteucci 2003; Carigi et al. 2002; Cescutti et al. 2008), they mainly targeted intermediate-mass elements and Fe because there were only a few samples of Mn at that time. Now, Mn has become one of the most observed elements in local dSphs among the iron-peak elements. The results of N12 show that the data distribution is disperse and quite different for different dSphs, so using a usual single theoretical curve to describe such distributions is not suitable. Up to now, how

Table 1 The parameters used for the three local dSphs, where α, λ and λ_* are from QW12, and α', λ' and λ'_* are from our model calculations (Fig. 1).

dSph	M_0 ($M_\odot$)	α	α'	λ	λ'	λ_*	λ'_*
Fornax	4.76E+8	1.00	5.00	1.05	1.30	0.069	0.345
Sculptor	8.16E+7	−1.00	0.00	0.70	0.70	0.018	0.062
Sextans	6.12E+7	−0.55	1.00	0.80	0.80	0.019	0.029

to understand the observational results is still an unsolved problem. Previous studies (see e.g. Cescutti et al. 2008; Romano & Starkenburg 2013; N12) show that it is not easy to explain the Mn distribution in dSphs self-consistently. Cescutti et al. (2008) and N12 adopted the assumption of metal-dependent Mn yield for Type Ia supernovae (SNeIa). Romano & Starkenburg (2013)'s results indicate that distributions of Fe and Mn are difficult to satisfy by one model simultaneously. In this paper, we present a new method that is improved from a phenomenological model proposed by Qian & Wasserburg (2012, hereafter QW12). QW12 showed that their model can successfully describe most of the observed Fe distributions in local dSphs.

Here we further provide a reasonable explanation for the new observational data given by N12 for the dSphs Fornax, Sculpture and Sextans, and give a new theoretical model for more and more observational results of iron-peak elements in local dSphs.

2 MODEL DESCRIPTION

The origin of iron-peak elements is explosive silicon burning in both SNeIa and Core-Collapse supernovae (CCSNe). The evolution of iron-peak elements in dSphs is mainly influenced by three factors: evolution model of these dSphs, explosion rate of SNe and yields of SNe. We provide the details about them in the following.

2.1 Evolution Equations of dSphs and SFRs

As given by QW12, the evolution of Fe in a homogeneous system of condensed gas is governed by the following two equations:

$$\frac{dM_{\rm g}}{dt} = \left(\frac{dM_{\rm g}}{dt}\right)_{\rm in} - \psi(t) - F_{\rm out}(t), \quad (1)$$

$$\frac{dM_{\rm Fe}}{dt} = P_{\rm Fe}(t) - \frac{M_{\rm Fe}(t)}{M_{\rm g}(t)}[\psi(t) + F_{\rm out}(t)], \quad (2)$$

where t is the time starting from the formation of a galaxy, $M_{\rm g}(t)$ and $M_{\rm Fe}(t)$ are the masses of gas and Fe respectively in the galaxy at time t, $\psi(t)$ is the star formation rate (SFR), $F_{\rm out}(t) = (\lambda - \lambda_*)M_{\rm g}(t)$ is the rate of gas outflow, and $P_{\rm Fe}(t)$ is the net rate of Fe production in the system.

In Equation (1), $(dM_{\rm g}/dt)_{\rm in}$ is the infall rate of pristine gas. Assuming the SFR is proportional to the mass of gas (QW12), $\psi(t) = \lambda_* M_{\rm g}(t)$, where λ_* is a constant. In Equation (2), $P_{\rm Fe}(t) = \lambda_{\rm Fe} X_{\rm Fe}^{\odot} M_{\rm g}(t)$, where $\lambda_{\rm Fe}$ is assumed to be a constant by QW12 (i.e., an equivalent SNe yield used to represent the contributions from different types of SNe) and $X_{\rm Fe}^{\odot}$ is the mass fraction of Fe in the Sun.

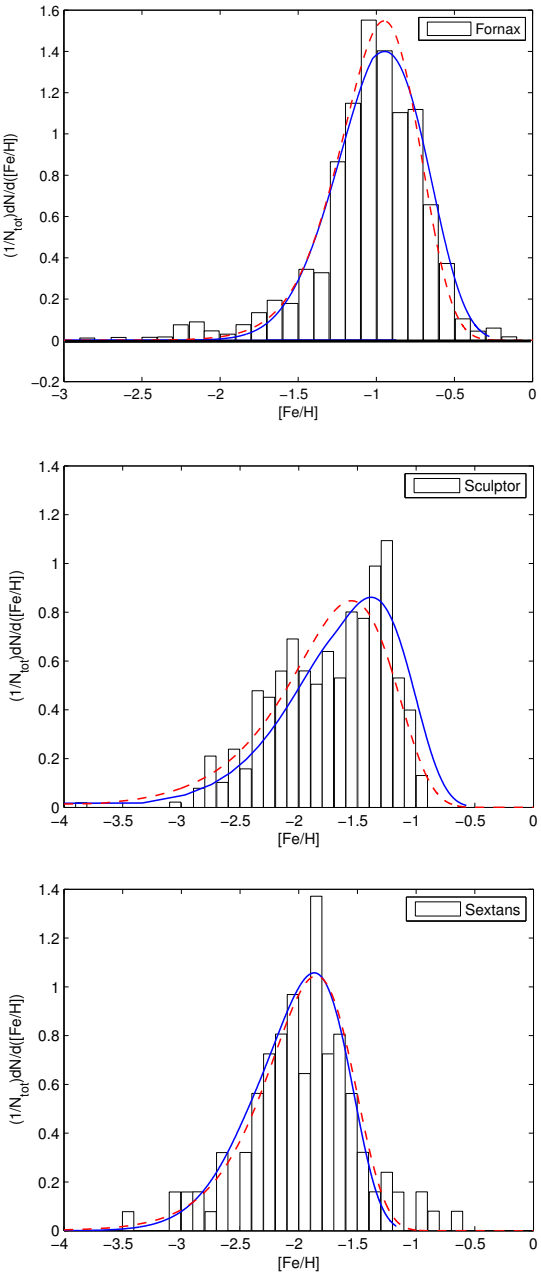

Fig. 1 Model fits (*solid curves*) to the observed metallicity (Fe) distributions (*histograms*) of the dSphs Fornax (*top*), Sculptor (*middle*) and Sextans (*bottom*; Kirby et al. 2011a). The model fits from QW12 are also shown (*dashed curves*) for comparison.

Equations (1) and (2) describe the budget for gas and Fe respectively. The gas (or Fe) mass in a system is equal to the infall rate of pristine gas (or the net yield of Fe) minus the mass consumed by star formation and the outflow driven by SNe. The solution of the above equations, i.e.,

the evolution of gas and Fe with time, has the following forms:

$$M_{\rm g}(t) \approx M_0 \frac{(\lambda t)^{\alpha+1}}{\Gamma(\alpha+2)} \exp(-\lambda t), \quad (3)$$

$$M_{\rm Fe}(t) \approx M_0 \frac{\lambda_{\rm Fe}}{\lambda} X_{\rm Fe}^{\odot} \frac{(\lambda t)^{\alpha+2}}{\Gamma(\alpha+3)} \exp(-\lambda t), \quad (4)$$

where $M_0 = (\Omega_{\rm b}/\Omega_{\rm m}) M_h = 0.17 M_h$; M_h is the total mass inside the dark matter halo hosting the system, and $\Omega_{\rm b}$ and $\Omega_{\rm m}$ are the fractional contributions to the critical density of the universe from baryonic and all matter, respectively. Γ is the gamma function, and λ and α are the parameters related to properties of each dSph, with their values found by matching the obtained metallicity distributions (QW12; see Table 1).

For example, λ and α determine the range of [Fe/H] and the height of the peak of the metallicity distribution, respectively. One important result from solving the equations is the SFR, which is described by a parameterized function as

$$\psi(t) \approx M_0 \lambda_* \frac{(\lambda t)^{\alpha+1}}{\Gamma(\alpha+2)} \exp(-\lambda t). \quad (5)$$

2.2 Model for Chemical Evolution of Mn

2.2.1 Evolution equations of Iron-peak elements

Since in addition to Fe, Mn is more easily observed than other iron-peak elements, it is thus used as an example to study the evolution of iron-peak elements. We modified QW12's model as follows: (i) QW12 considered the evolution of gas and iron, and we extend it to Mn; (ii) As already suggested by QW12, two types of SNe should be considered separately for the yields of iron-peak elements (QW12 lumped Fe together for simplification); (iii) SNe explosion rate is dependant on the SFR, but there is a time delay between a star's birth and death, which was ignored by QW12; (iv) The dependency of the SN yields on initial metallicity of stars is also taken into account in our model.

We modified Equation (2) by considering contributions from SNeIa and CCSNe separately in detail and including a time delay between the birth and death of SN progenitors. The evolution equation for Fe thus is

$$\frac{dM_{\rm Fe}}{dt} = P'_{\rm Fe}(t) - \frac{M_{\rm Fe}(t)}{M_{\rm g}(t)}[\psi(t) + F_{\rm out}(t)]. \quad (6)$$

In Equation (6), $P_{\rm Fe}(t)$ in Equation (2) is replaced by $P'_{\rm Fe}(t)$, where

$$P'_{\rm Fe}(t) = R_{\rm SNeIa}(t) y_{\rm Ia}^{\rm Fe}([{\rm Fe/H}]) + R_{\rm CCSNe}(t) y_{\rm CC}^{\rm Fe}([{\rm Fe/H}]).$$

$R_{\rm SNeIa}(t)$ and $R_{\rm CCSNe}(t)$ are the explosion rates for SNeIa and CCSNe at time t, respectively, and $R_{\rm SNe}(t) \propto \psi(t-\tau)$, where τ is the time delay. $y_{\rm Ia}^{\rm Fe}([{\rm Fe/H}])$ and $y_{\rm CC}^{\rm Fe}([{\rm Fe/H}])$ are the yields of Fe for SNeIa and CCSNe, respectively. [Fe/H] is the metallicity of progenitors. The forms of the SFR $\psi(t)$ and $F_{\rm out}(t)$ are the same as those in Equations (1)–(2), but their parameters are determined by the observed Fe distributions in the dSphs (see Fig. 1). The corresponding parameterized SFRs are shown in Figure 2. Note that those SFRs are not real SFRs. They are equivalent SFRs, by which we can reproduce the observed Fe distributions.

Similarly, the evolution equation for Mn is

$$\frac{dM_{\rm Mn}}{dt} = P'_{\rm Mn}(t) - \frac{M_{\rm Mn}(t)}{M_{\rm g}(t)}[\psi(t) + F_{\rm out}(t)], \quad (7)$$

where

$$P'_{\rm Mn}(t) = R_{\rm SNeIa}(t) y_{\rm Ia}^{\rm Mn}([{\rm Fe/H}]) + R_{\rm CCSNe}(t) y_{\rm CC}^{\rm Mn}([{\rm Fe/H}]).$$

where $y_{\rm Ia}^{\rm Mn}([{\rm Fe/H}])$ and $y_{\rm CC}^{\rm Mn}([{\rm Fe/H}])$ are the yields of Mn for SNeIa and CCSNe, respectively.

2.2.2 SNeIa explosion rate $R_{\rm SNeIa}$ and yields

SNeIa are generally regarded as thermonuclear explosions of accreting white dwarfs with high accretion rates. In such a white dwarf progenitor, relatively stable H and He shell burning is permitted, which leads to a growing C/O core. When the white dwarf's mass grows close to the Chandrasekhar mass, contraction sets in and the central density becomes high enough to ignite carbon fusion under degenerate conditions, inducing the thermonuclear explosion of the star (Brachwitz et al. 2000).

The SNIa explosion rate in a galaxy was first estimated by Greggio & Renzini (1983). While there are other different methods to calculate the SNIa rate, Greggio & Renzini (1983)'s method is still effective when coefficient A in Greggio & Renzini (1983)'s formula is adjusted slightly (Kobayashi & Nomoto 2009). Here following Greggio & Renzini (1983), we assumed that the lifetime of the progenitor binary of an SNIa is determined by the main-sequence time of the lower-mass star in the binary (companion star), and the SNIa rate is thus given by

$$R_{\rm SNeIa} = A \int_{m_{\rm min}^{\rm B}(t)}^{16} \varphi(M_{\rm B}) \int_{\mu_{\rm min}(t)}^{0.5} f(\mu) \psi(t-\tau_{\rm com}) d\mu dM_{\rm B}, \quad (8)$$

where A is a constant, and $A = 0.05$ is recommended for the general case (N12). The SNIa explosion rate in a galaxy is influenced by many factors, e.g., binary parameter (the fraction of primary stars that eventually explode as SNe Ia for RG+WD and MS+WD systems) (Kobayashi & Nomoto 2009), so $A = 0.05$ should not be suitable for every dSphs. Romano & Starkenburg (2013) applied $A = 0.03$, but we found that $A = 0.05$ for dSph Fornax, and $A = 0.02$ for Sextans and Sculptor are more suitable because these values can satisfy both the Mn and Fe distributions well. For comparison, we also show the results from $A = 0.03$ for Fornax. $M_{\rm B}$ is the total mass

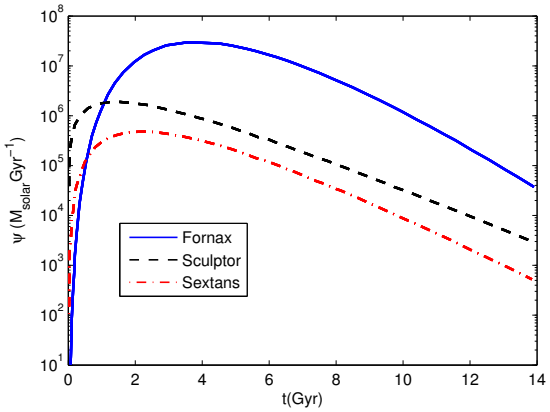

Fig. 2 SFHs for the dSphs Fornax, Sculptor and Sextans (*solid*, *dashed* and *dash-dotted* curves, respectively).

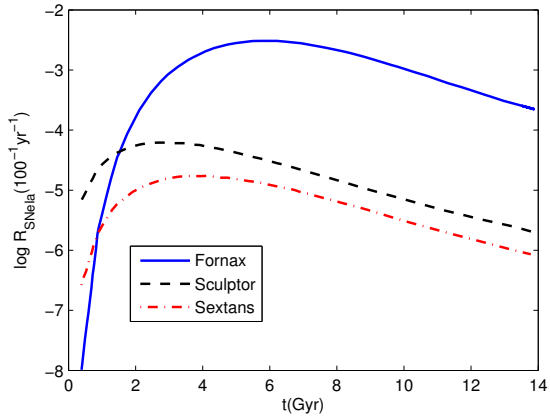

Fig. 3 Explosion rates of SNeIa as a function of time in the dSphs Fornax, Sculptor and Sextans (*solid*, *dashed* and *dash-dotted* curves, respectively.)

of the binary, $\varphi(M_{\rm B}) = \beta M_{\rm B}^{-(1+1.35)}$($\beta = 0.1716$; Tominaga et al. 2007) is the Salpeter initial mass distribution function, and $\tau_{\rm com}$ is the lifetime of the companion star in the binary, given by $\tau_{\rm com} = 5M_{\rm com}^{-2.7} + 0.012$ (for $M \leq 8\ M_{\odot}$). $m_{\rm min}^{\rm B}(t) = \max(2M_{\rm com}(t), 3)$, where $M_{\rm com}(t) = [(t - 0.012)/5]^{(-1/2.7)}$ is the minimal mass of the companion star at time t. Here we adopted the assumption in Matteucci & Greggio (1986) that the mass of an SNIa binary must be in the range of 3–16 $M_{\odot}$. In other words, only stars with mass larger than 1.5 $M_{\odot}$ but lower than 8 $M_{\odot}$ can finally form C/O white dwarfs. It can be noted that at very early epochs, a star with a mass of 1.5 $M_{\odot}$ has not finished its main-sequence evolution (1.685 Gyr is needed according to $\tau = 5M^{-2.7} + 0.012$). Therefore the minimal mass of the binary at early times is decided by the mass of the companion star that just ends its main-sequence evolution.

For example, at $t = 0.5$ Gyr, the minimal mass of a companion star is 2.36 $M_{\odot}$, and thus $m_{\rm min}^{\rm B}(0.5\ {\rm Gyr}) = 4.72\ M_{\odot}$. The factor 2 before $M_{\rm com}(t)$ implies that the total mass of the binary is at least two times larger than that of the companion star. $\mu = M_{\rm com}/M_{\rm B}$, and $f(\mu) = 24\mu^2$ is the distribution function for the mass fraction of the companion.

$$\mu_{\rm min}(t) = \max(M_{\rm com}(t)/M_{\rm B}, (M_{\rm B} - 8)/M_{\rm B})$$

is the minimum mass fraction contributing to the SNIa rate at time t.

Here the minimum mass of a companion star should be the larger one of these two values: (i) the minimal mass of a companion star which just ends its main-sequence evolution, or (ii) the mass of a binary minus the maximum mass of a C/O white dwarf progenitor (8 $M_{\odot}$). The explosion rates of SNeIa are shown in Figure 3.

Because the yields of SNeIa are a function of metallicity [Fe/H], and [Fe/H] is a function of t,

$$R_{\rm SNeIa}(t) y_{\rm Ia}([{\rm Fe/H}]) = A \int_{m_{\rm min}^{B}(t)}^{16} \varphi(M_{\rm B}) \int_{\mu_{\rm min}(t)}^{0.5} f(\mu)\psi (t - \tau_{\rm com}) y_{\rm Ia}^{\rm Mn}([{\rm Fe/H}]) d\mu dM_{\rm B}. \quad (9)$$

Although many authors (e.g., Nomoto et al. 1997; Iwamoto et al. 1999) carried out investigations, there are not systematic SN yields for progenitors with different metallicities. We used the yields of SNeIa given by Travaglio et al.

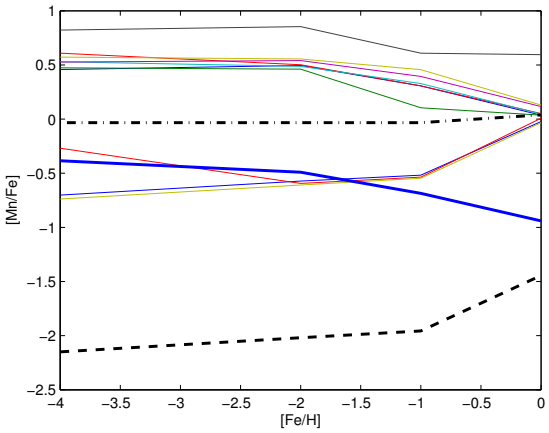

Fig. 4 [Mn/Fe] versus [Fe/H] for SNe of different progenitors. The top thin solid lines are for 12–25 $M_\odot$ CCSNe, and those below the thick dash-dotted line are results for 30, 35 and 40 $M_\odot$ CCSNe (WW95). The thick solid, dashed and dash-dotted lines are for 8.8 $M_\odot$ ONeMg SNe (Wanajo et al. 2009), 50 $M_\odot$ CCSNe (Tominaga et al. 2007) and SNeIa (Travaglio et al. 2005), respectively.

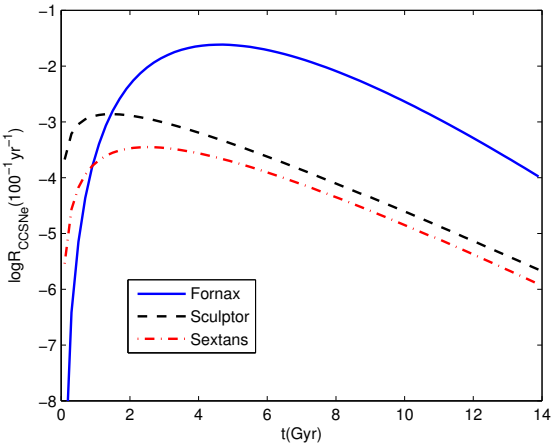

Fig. 5 Explosion rates of CCSNe as a function of time in the dSphs Fornax, Sculptor, and Sextans (*solid*, *dashed* and *dash-dotted* curves, respectively).

(2005), in which metallicities of $Z = 10^{-1}$, 1, 3 $Z_\odot$ are considered, where $Z_\odot$ is the solar metallicity. We also assumed that the Mn yield for SNeIa is metal-independent as $Z < 0.1\,Z_\odot$ (we will discuss this in Sect. 4) and used the interpolated values in the range of $Z = 0.1 - 3\,Z_\odot$. The thick dash-dotted line that varies slightly in Figure 4 shows the [Mn/Fe] distribution in detail.

2.2.3 CCSN explosion rate $R_{\rm CCSNe}$ and yields

Considering that stars with masses higher than 8 $M_\odot$ end as CCSNe, the explosion rate is equal to the number of dead massive stars

$$R_{\rm CCSNe} = \int_8^{100} \psi(t - \tau_m)\varphi(m)dm, \qquad (10)$$

where the lifetime τ_M for $M \geq 8\ M_\odot$ stars is

$$\tau_M = 1.2M^{-1.85} + 0.003.$$

In Figure 5, we show the CCSN explosion rates in the three dSphs calculated from the parameterized SFRs. The CCSN rates follow the SFRs closely since massive stars have short lifetimes, which can be seen in Figure 2 as variations of the rates are similar to those of their SFRs.

The explosion mechanism of CCSNe has been extensively studied, although there are still uncertainties. Current theories can explain low-energy CCSN explosions, such as ONeMg-core and some Fe-core progenitors, but it is still difficult for them to explain the most energetic CCSNe and hypernovae (Janka 2012). The yields of CCSNe strongly depend on the masses of progenitors. In the models of Woosley & Weaver (1995, hereafter WW95), only the mass range from 11 to 40 $M_\odot$ was considered. The WW95 models are generally consistent with the results from observational studies, but the yields are not strictly based on successful explosion models and the progenitors should be modified properly (Woosley et al.

2002). Adopting Salpeter's IMF and assuming all the 8–100 $M_\odot$ stars end their lives by CCSN explosions, the fractions of progenitor stars with 8–10 $M_\odot$ and >40 $M_\odot$ to the total number of CCSNe are 26.2% and 8.93% (the mass fractions are 12.2% and 43.66%), respectively. Thus both 8–10 $M_\odot$ ONeMg SNe and hypernovae should not be ignored. Including them, the contribution of CCSNe is given by

$$R_{\rm CCSNe}y_{\rm CC}([{\rm Fe/H}]) = \frac{\lambda_*}{\int_{0.1}^{100} m^{-1.35}dm} \times \left\{ \begin{array}{l} y_{8-10}([{\rm Fe/H}]) \int_8^{10} M_g(t-\tau_{\rm m})m^{-2.35}dm \\ +y_{10-12.5}([{\rm Fe/H}]) \int_{10}^{12.5} M_g(t-\tau_m)m^{-2.35}dm \\ +\ldots \\ +y_{45-100}([{\rm Fe/H}]) \int_{45}^{100} M_g(t-\tau_m)m^{-2.35}dm \end{array} \right\}, \quad (11)$$

where $y_{\rm number}([{\rm Fe/H}])$ denotes the yields and the subscripts are the mass ranges of progenitors. In our calculation, the mass range of 8 $M_\odot$–100 $M_\odot$ was divided into 12 sub-ranges, with the following progenitor models used: 8.8, 12, 13, 15, 18, 20, 22, 25, 30, 35, 40 and 50 $M_\odot$. The nucleosynthesis yields of the 8.8 $M_\odot$ model was used for the presupernova whose mass range is 8–10 $M_\odot$, that of 12 $M_\odot$ model for the presupernova whose mass range is 10–12.5 $M_\odot$, and so forth. The values of the nucleosynthesis yields of 8.8 $M_\odot$ and 11–40 $M_\odot$ SNe were from the standard model of Wanajo et al. (2009) and WW95, respectively, while those of 50 $M_\odot$ SNe were from the standard model 50A in Tominaga et al. (2007). Yields with different [Fe/H] from $Z = 0$ to $Z_\odot$ were provided for 11–40 $M_\odot$ models in WW95, but Wanajo et al. (2009) only provided the yields of 8.8 $M_\odot$ for the progenitor with solar metallicity and Tominaga et al. (2007) provided those for 50 $M_\odot$ with zero metalicity. Therefore we assumed that the Mn/Fe slope is the same as those in the 15A and 40A models of WW95 for 8.8 $M_\odot$ and the 50A model, respectively (shown in Fig. 4). WW95 provided 2–3 different models for masses of 30, 35 and 40 $M_\odot$. We found that [Mn/Fe] of the B or C model in WW95 varied abruptly, so we used the 30A, 35A and 40A models. As shown in Figure 4, [Mn/Fe] of WW95 decreases with [Fe/H] for models 12–25 $M_\odot$, but the case reverses for the models with 30–40 $M_\odot$. It can also be noted that [Mn/Fe] of WW95 is generally larger than that of the other cases of CCSNe.

3 RESULTS

Including detailed calculations of the explosion rates and yields of the two types of SNe, we solved Equations (1), (5), (6), (9) and (11). The SFR parameters α, λ and λ_* in the equations were replaced by α', λ' and λ'_*, respectively, in our calculations. The values for α', λ' and λ'_* are given in Table 1. These parameters were adjusted to describe the observed Fe distributions of the dSphs Fornax, Sculptor and Sextans (Kirby et al. 2011a). One can find from Figure 1 that our parameters (solid lines) describe the bulk of the Fe distribution quite well. Because the curves are normalized, they cannot satisfy the height and width of the peak simultaneously. As a comparison, the model fits from QW12 are also shown (dashed lines).

In Figures 6–8 we show the resultant [Mn/Fe] ratio curves as a function of [Fe/H] for the three dSphs. The observational samples are from N12 and Shetrone et al. (2003), which are plotted as circular and square data points respectively (two samples denoted by the squares in Sextans may not be reliable according to the authors). Theoretical data from Romano & Starkenburg (2013)'s models are also plotted as colored dots. The dashed, dash-dotted, and thick solid curves are the results considering the contributions from SNeIa, CCSNe and the sum of them respectively. Note that [Fe/H] essentially represents t. It can be seen that the trends of the [Mn/Fe] curves representing the three local dSphs are similar: they decrease with time at the beginning (It is the apparent reason for the samples with high [Mn/Fe] at low [Fe/H], which was not explained by previous studies.), and then rise gently. At low/high [Fe/H], the solid curves are close to the dash-dotted/dashed curves, respectively. The reason is that at the early stage, CCSNe are the main explosions, but as the number of massive stars becomes less and less at the late stage of dSphs, the yield of Mn is then dominated by SNeIa.

The curves of SNeIa are generally higher than the observational values, but the case reverses for those of the CCSNe. Some samples are close to curves of SNeIa, suggesting that the primeval gases that form these stars are relics of SNeIa. Similarly, samples that are close to the curves of CCSNe probably acquired their primeval gas from CCSNe explosions. For most of the samples, their primeval gas should have been from both of these two types of SNe. Thus they are located between the dashed and dash-dotted curves, and approximately around the thick solid curve. The total number of samples is 161 in three figures (80 for dSph Sculptor, 74 for dSph Fornax and 7 for dSph Sextans). Only two samples in the dSph Sculptor are outside of our model curves. Therefore our model can generally describe the distributions of the Mn abundance in the dSphs.

It can also be noted that the model curves for Fornax describe the data better than for Sculptor. The possible reason is that the metallicity distribution of Fornax is clearly single-peaked, while that of Sculptor may contain two components. Our model (or the QW12 model), which is rather simplified, is built to describe single-peaked cases. The two-peaked distribution, if confirmed by further observations, may imply a more complicated evolution history for the galaxy.

4 DISCUSSION

4.1 Initial [Mn/Fe]

Comparing with previous results (e.g., figs. 1 and 2 in Cescutti et al. 2008 or N12), their [Mn/Fe] ratio curves rise

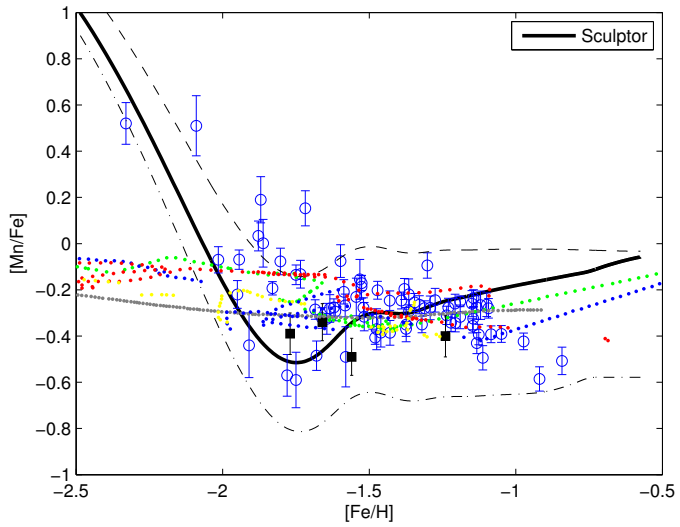

Fig. 6 [Mn/Fe] versus [Fe/H] for the dSph Sculptor. The circles and squares are the measurements from N12 and Shetrone et al. (2003), respectively. The colored dots are theoretical predictions from Romano & Starkenburg (2013)'s models. The dashed, dash-dotted and solid curves are the contributions from SNeIa, CCSNe and both of them, respectively, resulting from our model calculation.

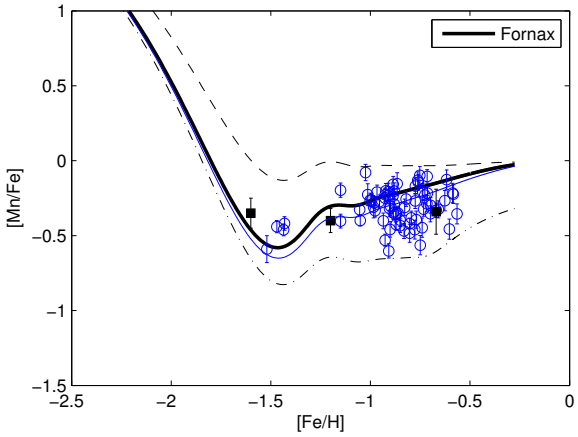

Fig. 7 [Mn/Fe] versus [Fe/H] for the dSph Fornax. Symbols and curves are the same as in Fig. 6. The thin solid curve is the result considering $A = 0.03$ and the contributions from two types of SNe.

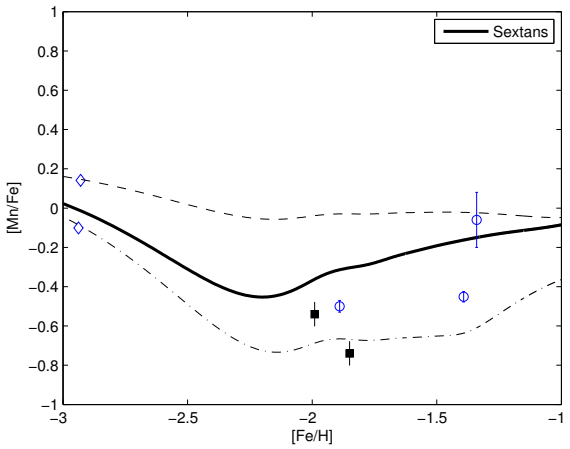

Fig. 8 [Mn/Fe] versus [Fe/H] for the dSph Sextans. The diamonds are the measurements from Tafelmeyer et al. (2010), and other symbols and curves are the same as in Fig. 6.

at the initial stage, which is opposite to ours. This difference is caused by the initial [Mn/Fe]. Usually stars with masses lower than 100 $M_\odot$ are only included in the calculations. However if we consider that a very small number of supermassive stars ($> 100\ M_\odot$) explode at the very early time, the initial [Mn/Fe] should be set by these supermassive stars, whose values of [Mn/Fe] are very small (e.g., [Mn/Fe] ≈ -1.5 for solar metallicity progenitors according to Tominaga et al. 2007).

In fact, the number of these supermassive stars is too small to have any effects on the evolution of galaxies according to theoretical estimation, and we assumed both the initial Mn and Fe are nearly equal to zero for Sculptor and Fornax. According to the definition

$$[\mathrm{Mn/Fe}] \equiv \log(M_{\mathrm{Mn}}/M_{\mathrm{Fe}})/(M_{\mathrm{Mn}\odot}/M_{\mathrm{Fe}\odot}),$$

$[\mathrm{Mn/Fe}]_{\mathrm{ini}} = 1.96$ can be set. This initial value results in the downward trend in the early time, which naturally explains the observed star samples in the dSphs, particularly in Sculptor. However for the dSph sextans, there are two samples with [Fe/H] $= -2.9$ (plotted as diamonds in Fig. 8). They can be explained as the initial [Mn/Fe] is 0.36 (see Fig. 8). This means that the data before the minimum point indicate the primeval [Mn/Fe] of dSphs. In other words, a ratio curve before its minimum point is highly determined by the initial [Mn/Fe] condition.

4.2 Weak Metal-Dependent [Mn/Fe] of SNeIa?

Some previous authors have assumed that the Mn yield of SNeIa is proportional to the progenitor metallicity by $y_{\rm Mn}(z) \propto (\frac{Z}{Z_\odot})^{0.65}$, in order to have results consistent with the observational data (see e.g., Cescutti et al. 2008). This is a strong [Mn/Fe]-[Fe/H] relationship. In our calculation, we adopted the nucleosynthesis network results of Travaglio et al. (2005), in which the Mn yield is 5.15×10^{-3}, 6.38×10^{-3} and 9.19×10^{-3} $M_\odot$, corresponding to progenitor metallicity 0.1, 1 and 3 $Z_\odot$ respectively. One can find that this is much weaker than the previously assumed metal-dependent relation. Because there is a significant time delay due to the SNIa progenitor evolution, the metallicity of most of the SNIa progenitors in the dSphs is less than $0.1\ Z_\odot$.

For the case of [Fe/H] < -1 (i.e., metallicity $< 0.1\ Z_\odot$), we used the same Mn yields as the case of progenitor metallicity $[{\rm Fe/H}] = -1$. The results are much better than the case using the assumption of Cescutti et al. (2008). We note that while the metallicity dependence of SNIa yields is not included in Kobayashi & Nomoto (2009)'s model, their model can give a better reproduction of the [(α, Mn, Zn)/Fe]$-$[Fe/H] relations in the solar neighborhood than other models. Our calculation is thus in line with theirs. The previous authors usually use the yields of 11–40 $M_\odot$ SNe whose Mn fraction is generally high (see Fig. 4). In order to be consistent with observational results, the Mn yield of SNeIa therefore has to be reduced. Our calculation included more CCSNe subtypes, such as 8.8 and 50 $M_\odot$ SNe, whose [Mn/Fe] fraction is quite low (see Fig. 4). This removes the need for the previous assumption.

5 CONCLUSIONS

Including detailed calculations for the SNe explosion rates and yields of different types of SNe, we have developed a model for the chemical evolution of iron-peak elements in dSphs. We have shown that our model can successfully explain the currently observed Mn abundance in the stars of three dSphs, suggesting its effectiveness. As studies of dSphs are being conducted with current large telescopes and will continue with extremely large facilities in the near future such as the Thirty Meter Telescope, our model could be further tested and modified if required. In addition, although it is generally very difficult to measure other low abundance iron-peak elements, our model should be suitable for them. One only needs to replace Mn with the element of interest. Following this work, we will consider incorporating SFRs derived from color-magnitude diagrams (e.g., de Boer et al. 2012), which will probably be able to provide more information about the evolution processes in dSphs.

Acknowledgements MQL would like to thank professor Y. Z. Qian at the University of Minnesota for his useful discussion. This work is partly supported by the National Natural Science Foundation of China (Grant Nos. 11305133, 11273020 and U1331121) and China Scholarship (Grant No. 2011851096).

References

Bhattacherjee, B., Ibe, M., Ichikawa, K., Matsumoto, S., & Nishiyama, K. 2014, Journal of High Energy Physics, 7, 80
Brachwitz, F., Dean, D. J., Hix, W. R., et al. 2000, ApJ, 536, 934
Carigi, L., Hernandez, X., & Gilmore, G. 2002, MNRAS, 334, 117
Cescutti, G., Matteucci, F., Lanfranchi, G. A., & McWilliam, A. 2008, A&A, 491, 401
de Boer, T. J. L., Tolstoy, E., Hill, V., et al. 2012, A&A, 544, A73
Graziani, L., Salvadori, S., Schneider, R., et al. 2015, MNRAS, 449, 3137
Greggio, L., & Renzini, A. 1983, A&A, 118, 217
Helmi, A., Irwin, M. J., Tolstoy, E., et al. 2006, ApJ, 651, L121
Iwamoto, K., Brachwitz, F., Nomoto, K., et al. 1999, ApJS, 125, 439
Janka, H.-T. 2012, Annual Review of Nuclear and Particle Science, 62, 407
Kirby, E. N., Lanfranchi, G. A., Simon, J. D., Cohen, J. G., & Guhathakurta, P. 2011a, ApJ, 727, 78
Kirby, E. N., Martin, C. L., & Finlator, K. 2011b, ApJ, 742, L25
Kobayashi, C., & Nomoto, K. 2009, ApJ, 707, 1466
Lanfranchi, G. A., & Matteucci, F. 2003, MNRAS, 345, 71
Matteucci, F., & Greggio, L. 1986, A&A, 154, 279
Nomoto, K., Iwamoto, K., Nakasato, N., et al. 1997, Nuclear Physics A, 621, 467
North, P., Cescutti, G., Jablonka, P., et al. 2012, A&A, 541, A45
Qian, Y.-Z., & Wasserburg, G. J. 2012, Proceedings of the National Academy of Science, 109, 4750
Romano, D., & Starkenburg, E. 2013, MNRAS, 434, 471
Shetrone, M., Venn, K. A., Tolstoy, E., et al. 2003, AJ, 125, 684
Tafelmeyer, M., Jablonka, P., Hill, V., et al. 2010, A&A, 524, A58
Tolstoy, E., Hill, V., & Tosi, M. 2009, ARA&A, 47, 371
Tominaga, N., Umeda, H., & Nomoto, K. 2007, ApJ, 660, 516
Travaglio, C., Hillebrandt, W., & Reinecke, M. 2005, A&A, 443, 1007
Wanajo, S., Nomoto, K., Janka, H.-T., Kitaura, F. S., & Müller, B. 2009, ApJ, 695, 208
Woosley, S. E., Heger, A., & Weaver, T. A. 2002, Reviews of Modern Physics, 74, 1015
Woosley, S. E., & Weaver, T. A. 1995, ApJS, 101, 181